

Downwash-aware Control Allocation for Over-actuated UAV Platforms

Yao Su^{1*}, Chi Chu^{1,2*}, Meng Wang¹, Jiarui Li^{1,3}, Liu Yang^{1,4}, Yixin Zhu⁵, Hangxin Liu^{1†}

Abstract— Tracking position and orientation independently affords more agile maneuver for over-actuated multirotor Unmanned Aerial Vehicles (UAVs) while introducing undesired downwash effects; downwash flows generated by thrust generators may counteract others due to close proximity, which significantly threatens the stability of the platform. The complexity of modeling aerodynamic airflow challenges control algorithms from properly compensating for such a side effect. Leveraging the input redundancies in over-actuated UAVs, we tackle this issue with a novel control allocation framework that considers downwash effects and explores the entire allocation space for an optimal solution. This optimal solution avoids downwash effects while providing high thrust efficiency within the hardware constraints. To the best of our knowledge, ours is the first formal derivation to investigate the downwash effects on over-actuated UAVs. We verify our framework on different hardware configurations in both simulation and experiment.

I. INTRODUCTION

Over-actuated UAV platforms with independent position and orientation tracking provide more agile maneuver compared with traditional multirotors. A straightforward realization is to tilt propellers [1–4] and generate thrust forces in non-collinear directions. As a result, many platforms employ **actively tiltable thrust generators** [5–7], achieving higher thrust efficiency and enabling omnidirectional flights [3, 7].

Adopting tiltable thrust generators unfortunately also introduces a common side effect—the downwash effect [8], which has been rarely studied in the context of over-actuated UAVs. This effect occurs when the airflow generated by one thrust generator/propeller passes through and interacts with other(s), resulting in deteriorated trajectory tracking performance and lower trust efficiency; illustrated in Fig. 1. In the literature, the downwash effects are primarily treated by compensation [9–13] or as disturbances to be slowly attenuated by adding integrators into trajectory tracking controller [7, 14]. However, the former approach needs numerous experimental data to learn the platform-specific compensator, which cannot be generalized to other platforms. The latter solution is slow in response, and hence has undesirable transitional behavior (*e.g.*, obvious drop in the flow direction). Critically, both approaches only handle the downwash effect

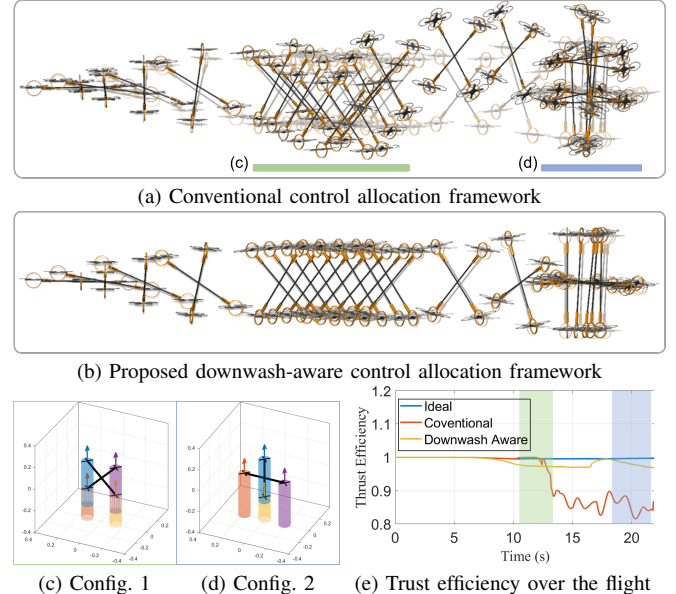


Fig. 1: Comparison between the proposed control allocation framework with conventional ones when tracking the reference trajectory indicated by the light grey. (a) Conventional control allocation framework fails to track stably as downwash effects appear twice, highlighted in green and blue. Exemplar configurations solved by the conventional control allocation framework may lead to (c) two and (d) one pair of downwash effects, where arrows and cylinders stand for the thrust forces and downwash flows, respectively. (b) The proposed framework avoids downwash effects and thus maintains both stable tracking performance and high trust efficiency over the challenging flight. (e) We further compare the trust efficiency of ideal (the reference trajectory), conventional, and our proposed allocation frameworks.

after it occurs and are *inefficient* in terms of energy, requiring extra thrusts to compensate.

In this paper, we tackle the downwash effects from a novel control allocation perspective for over-actuated UAVs with actively tiltable thrust generators. Due to input redundancy, there exists an infinite number of solutions to allocate desired force and torque commands to the low-level commands of thrust generators. This observation makes it possible to find a proper allocation such that no air flows would counteract with other thrust generators through a flight, thus reducing or even eliminating downwash effects *beforehand*.

To realize this idea, we first incorporate the aerodynamics model for downwash effect analysis and investigate the relationship between **downwash effect avoidance** and **thrust efficiency**. Next, we extend our nullspace-based control allocation framework [14] by adding downwash avoidance constraints and a thrust efficiency index in the objective function. In simulation, we verify the proposed downwash-aware

* Yao Su and Chi Chu contributed equally to this work.

¹ Beijing Institute for General Artificial Intelligence (BIGAI). Emails: {suyao, chuchi, wangmeng, lijiaru, yangliu, liuhx}@bigai.ai.

² Department of Automation, Tsinghua University.

³ College of Engineering, Peking University.

⁴ Academy of Arts & Design, Tsinghua University.

⁵ Institute for Artificial Intelligence and School of Artificial Intelligence, Peking University. Email: yixin.zhu@pku.edu.cn.

† Corresponding author.

control allocation framework on different over-actuated UAV platforms. In experiment, we build physical platforms that combine commercial quadcopters with passive gimbal joints as 3-Degree of Freedom (DoF) thrust generators and verify the proposed framework. Collectively, we demonstrate that the proposed framework can fully explore the entire allocation space and find the optimal allocation solution that avoids downwash effects and maintains a high thrust efficiency.

A. Related Work

Downwash effects have recently drawn research attention, primarily on computational models of two UAVs [15–17] to achieve better motion cooperation [18, 19]. Downwash effects for multi-UAV systems are more challenging to handle. The most straightforward solution is to keep enough safety distance among UAVs to avoid the interference introduced by downwash effects [20]. Learning-based method has also been proposed to compensate for the downwash effects among multirobot swarm [21, 22]. Different from the above work in multi-agent scenarios, we study over-actuated UAV platforms, wherein several thrust generators are physically connected to a common frame. By developing a centralized control allocation framework, our framework avoids the downwash effects by exploiting input redundancy when generating low-level control commands of thrust generators.

Commanding each actuator given the desired total wrench of the platform, the **control allocation** of over-actuated UAV platforms is a constrained nonlinear optimization problem and generally difficult to solve with high efficiency. Prior works leverages gradient-descent [23], force decomposition [24], iterative approach [25], separation method [26], and linear approximation [27] to reduce the computational complexity. However, none can incorporate input constraints while providing exact solutions with satisfied efficiency. This limitation was first solved by Su *et al.* [14], who devised a *nullspace-based* control allocation framework; henceforth, we referred to this framework as the **conventional allocation framework**. In this paper, we extend this framework by incorporating a downwash effect avoidance constraint and adding a thrust efficiency index in the objective function. As a result, various UAV platforms with 3-DoF thrust generators [1–4, 7, 28] can achieve any arbitrary attitude without downwash effects while maintaining high thrust efficiency along the entire possible configuration space.

B. Overview

We organize the remainder of the paper as follows. Section II presents the dynamics model of the UAV system with downwash effect modeling. We analyze downwash effects and study the relation between downwash effect avoidance and thrust efficiency in Section III. Section IV describes the hierarchical control structure and the proposed downwash-aware allocation framework. Section V and Section VI show the simulation and experiment results with comprehensive evaluations. Finally, we conclude the paper in Section VII.

II. PLATFORM MODEL WITH AERODYNAMICS

The over-actuated UAV system discussed in this paper adopts regular quadcopters with 2-DoF passive gimbal mech-

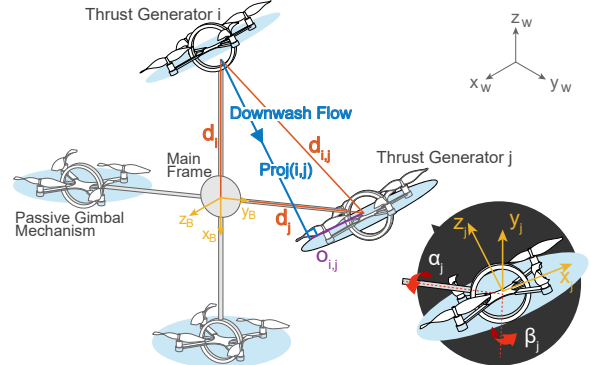


Fig. 2: **Coordinate systems of the over-actuated UAV platform.** Regular quadcopters are connected to the mainframe by 2-DoF passive gimbal mechanism, serving as 3-DoF thrust generators. Each quadcopter generates downwash flow in thrust's opposite direction.

anism, serving as 3-DoF thrust generators [7]. This system has demonstrated various configurations depending on the number of thrust generators and mainframe design [29], and its dynamics is mathematically equivalent to some semimal platforms [2–4, 7].

A. System Frames and Configuration

Fig. 2 outlines the system frames and configurations. Let \mathcal{F}_W denote the world coordinate frame and attach the platform frame \mathcal{F}_B to the geometric center of the UAV platform. We define the central position of the main frame as $\xi = [x, y, z]^T$, the attitude in the roll-pitch-yaw convention as $\eta = [\phi, \theta, \psi]^T$, and the platform angular velocity in \mathcal{F}_B as $\nu = [p, q, r]^T$. Actuator frames \mathcal{F}_i s are attached to the geometric center of the i th 3-DoF thrust generator.

B. Platform Dynamics

The dynamics model of this over-actuated UAV platform can be described as in Yu *et al.* [7].

$$\begin{bmatrix} m^{\{W\}} \ddot{\xi} \\ \{B\} J^{\{B\}} \ddot{\nu} \end{bmatrix} = \begin{bmatrix} {}^{\{W\}} R_{\{B\}} & 0 \\ 0 & I_3 \end{bmatrix} \mathbf{u} + \begin{bmatrix} mg \hat{\mathbf{z}} \\ {}^{\{B\}} \boldsymbol{\tau}_g \end{bmatrix} + {}^{ext} \mathbf{u}, \quad (1)$$

where the translational dynamics are expressed in the world frame \mathcal{F}_W , whereas the rotational dynamics are described in body-fix frame \mathcal{F}_B . m and J are the total mass and inertia matrix of the platform, respectively. $\ddot{\xi}$ and $\ddot{\nu}$ are the linear and angular acceleration of the central frame, respectively. g is the acceleration due to gravity, ${}^{\{B\}} \boldsymbol{\tau}_g$ is the gravity torque due to the displacement of its center of mass (CoM) from the geometric center [3], $\hat{\mathbf{z}} = [0, 0, 1]^T$, and

$$\mathbf{u} = \begin{bmatrix} \sum_{i=1}^N {}^{\{B\}} R_{\{i\}} T_i \hat{\mathbf{z}} \\ \sum_{i=1}^N (\mathbf{d}_i \times {}^{\{B\}} R_{\{i\}} T_i \hat{\mathbf{z}}) \end{bmatrix} = \begin{bmatrix} \mathbf{J}_\xi(\alpha, \beta) \\ \mathbf{J}_\nu(\alpha, \beta) \end{bmatrix} \mathbf{T}, \quad (2)$$

where T_i , α_i , and β_i denote the magnitude of thrust, tilting, and twisting angles of the i th thrust generator. N is the number of thrust generators, \mathbf{d}_i the distance vector from \mathcal{F}_B 's center to each \mathcal{F}_i , and ${}^{ext} \mathbf{u}$ the external force/torque input, assumed to be caused by downwash effects.

C. Downwash Effect Modeling

As elaborated by Khan *et al.* [15], for the zone of flow establishment (ZFE), the velocity field of a quadcopter

follows a Gaussian distribution,

$$V(z, r) = V_{ZFE,max}(z) e^{-\frac{1}{2} \left(\frac{r-R_{m0}}{0.5R_{m0}+0.075(z-z_0-R_0)/K_{visc}} \right)^2}, \quad (3)$$

with

$$V_{ZFE,max}(z) = V_0 [c_1 - c_2 K_{visc}(z - z_0)/R_0], \quad (4)$$

where z and r are the vertical and radial separations, respectively. K_{visc} is the viscosity constant. z_0 , R_0 , and V_0 are the position, contracted radius, and induced velocity of the efflux plane, respectively. R_{m0} is the radial location of the maximum velocity at each cross-section. c_1 and c_2 are two parameters, which can be experimentally determined.

With the model introduced in [17], the thrust change caused by oncoming flows for every propeller is estimated:

$$\Delta t_{i,j} = -b_v \sum_{k=1}^N V(z_{i,j,k}, r_{i,j,k}) t_{i,j}, \quad \forall j = 1, \dots, 4 \quad (5)$$

where $t_{i,j}$ is the thrust generated by the j th propeller of i th quadcopter module, defined by:

$$t_{i,j} = K_T \omega_{i,j}^2, \quad (6)$$

where $\omega_{i,j}$ is the rotational speed. $z_{i,j,k}$ and $r_{i,j,k}$ are the vertical and radial separations between i th quadcopter's j th propeller and k th quadcopter's downwash flow. b_v is the thrust decay coefficient, obtained experimentally.

Now we can calculate the thrust and torque disturbance of the i th quadcopter caused by the downwash effects as [30]

$$\begin{bmatrix} \Delta T_i \\ \Delta M_i \end{bmatrix} = \begin{bmatrix} 1 & 1 & 1 & 1 \\ b & -b & -b & b \\ -b & -b & b & b \\ -c_\tau & c_\tau & -c_\tau & c_\tau \end{bmatrix} \begin{bmatrix} \Delta t_{i,1} \\ \Delta t_{i,2} \\ \Delta t_{i,3} \\ \Delta t_{i,4} \end{bmatrix}, \quad (7)$$

where ΔM_i affects the low-level attitude control of i th quadcopter. $M_i = [M_i^x, M_i^y, M_i^z]^\top$ are the torque outputs in \mathcal{F}_i . b is a constant defined as $b = a/\sqrt{2}$, where a is the distance of each propeller to the quadcopter center. c_τ is a constant defined as $c_\tau = K_\tau/K_T$, where K_τ is the propeller drag constant, and K_T the standard propeller thrust constant. ΔT_i mainly influences the high-level control as external force, and we can have

$${}^{ext}\mathbf{u} = \begin{bmatrix} {}^W\mathbf{R}_{\{B\}} (\sum_{i=1}^N {}^B\mathbf{R}_{\{i\}} \Delta T_i \hat{\mathbf{z}}) \\ \sum_{i=1}^N (\mathbf{d}_i \times {}^B\mathbf{R}_{\{i\}} \Delta T_i \hat{\mathbf{z}}) \end{bmatrix}. \quad (8)$$

Section VI adopts this downwash effect model for simulation with the parameters acquired from experimental data.

III. DOWNWASH EFFECT ANALYSIS

A. Downwash Constraint Derivation

As shown in Fig. 2, the radial distance between i th quadcopter's downwash flow and j th quadcopter's center is defined as $O_{i,j}$, which be calculated by

$$O_{i,j} = \sqrt{\|\mathbf{d}_{i,j}\|^2 - \|proj(i, j)\|^2}, \quad (9)$$

$$\mathbf{d}_{i,j} = \mathbf{d}_j - \mathbf{d}_i, \quad (10)$$

$$proj(i, j) = dot(\mathbf{d}_{i,j}, {}^B\mathbf{R}_{\{i\}} \hat{\mathbf{z}}), \quad (11)$$

where dot refers to the dot product of two vectors. By having ${}^B\mathbf{R}_{\{i\}}$, $O_{i,j}$ is a function of α_i and β_i . If we build a vector

Algorithm 1: Downwash Constraint Calculation

```

Data:  $d_i, {}^B\mathbf{R}_{\{i\}}, N, o_{min}$  constant
Result:  $O_{min}$ 
i  $\leftarrow 1, j \leftarrow 2, k \leftarrow 0;$ 
 $O_{min} \leftarrow zeros(N(N-1), 1);$ 
for  $i = 1 \dots N$  do
    for  $j = 1 \dots N$  do
        if  $i \neq j$  then
             $k \leftarrow k + 1;$ 
             $d_{i,j} \leftarrow \mathbf{d}_j - \mathbf{d}_i;$ 
             $proj(i, j) \leftarrow dot(d_{i,j}, {}^B\mathbf{R}_{\{i\}} \hat{\mathbf{z}});$ 
            if  $proj(i, j) \leqslant 0$  then
                 $O_{min}(k) \leftarrow 0$ 
            else
                 $O_{min}(k) \leftarrow o_{min}^2$ 
            end
        end
    end
end

```

$\mathbf{O}(\alpha, \beta) = [O_{1,2}^2; \dots; O_{N,N-1}^2] \in \mathbb{R}^{N(N-1) \times 1}$ by stacking $O_{i,j}^2$, we can calculate a minimum distance vector O_{min} to constraint \mathbf{O} . As a result, the downwash effect avoidance can be achieved by requiring

$$\mathbf{O}(\alpha, \beta) \geqslant O_{min}. \quad (12)$$

Of note, as shown in Algorithm 1, we need only this constraint when the downwash flows go through other quadcopters in the positive direction. As this inequality constraint is highly nonlinear, we approximately include this constraint into the nullspace-based allocation framework by first-order linearization, to be detailed in Section IV-B.

B. Downwash Effect Avoidance and Thrust Efficiency

The “thrust efficiency index” was defined by Ryll *et al.* [31] to quantify wasted internal forces in over-actuated multirotor systems. Formally, it is defined as

$$\begin{aligned} \eta_f &= \frac{\|\sum_{i=1}^N {}^B\mathbf{R}_{\{i\}} T_i \hat{\mathbf{z}}\|}{\sum_{i=1}^N T_i} = \frac{\|\mathbf{J}_\xi(\alpha, \beta) \mathbf{T}\|}{\sum_{i=1}^N T_i} \\ &= \frac{\|\mathbf{u}(1 : 3, 1)\|}{\sum_{i=1}^N T_i}, \quad \eta_f \in [0, 1] \end{aligned} \quad (13)$$

where η_f is a configuration-dependent ratio between the sum of vectored thrusts and the sum of total thrust magnitudes.

We study the relation between downwash avoidance and thrust efficiency for three different over-actuated UAV configurations—platforms with four, five, and six 3-DoF thrust generators; Fig. 3 summarizes the results. When the platforms fly vertically (see Figs. 3a, 3d and 3g), downwash effects still appear as most prior allocation frameworks [7, 14] if we only try to maintain maximum thrust efficiency ($\eta_f = 1$). By exploring the entire configuration space, other feasible configurations might both avoid downwash effects and maintain high thrust efficiency (see Figs. 3c, 3f and 3i). This finding motivates us to propose a new allocation framework that efficiently finds such a configuration for the over-actuated UAV platforms at each timestep.

In Eq. (13), the numerator of η_f is provided by wrench command \mathbf{u} of tracking controller, which can be treated as

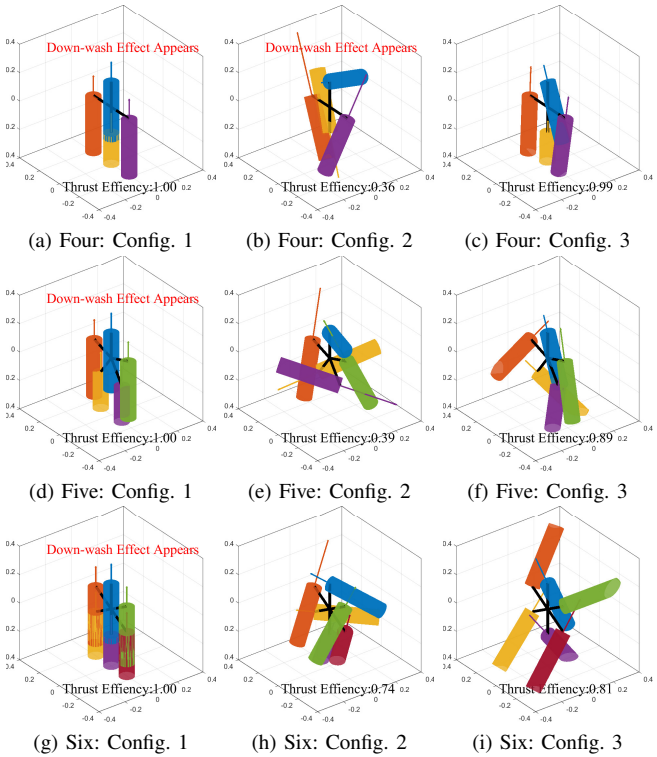


Fig. 3: Thrust efficiency and downwash effect avoidance for different over-actuated UAV platforms. Infinite number of thrust force combinations can generate same required wrench command with different thrust efficiencies. For each platform, three configurations are provided as examples. Four, five, six refer to the platform with 4, 5, or 6 3-DoF thrust generators, respectively. Henceforth, we use the same notations for the number of thrust generations in the platform.

a constant value in allocation. To include thrust efficiency index into the objective function of the nullspace-based allocation framework, we choose to minimize the denominator of Eq. (13) ($\sum_{i=1}^N T_i$); please refer to Section IV-B for details.

IV. DOWNWASH-AWARE CONTROLLER DESIGN

The overall controller has a hierarchical architecture, shown in Fig. 4. The high-level trajectory tracking controller (see Fig. 4a) (i) calculates the desired force/torque command (6-DoF wrench command) for the whole platform, and (ii) allocates the force/torque command to tilting angle α_i , twisting angle β_i , and thrust T_i of each 3-DoF thrust generator. The low-level controller (see Fig. 4b) of each quadcopter (i) regulates the individual attitude to the desired values and (ii) provides the required thrust force.

A. High-level Control

Without downwash effects, the dynamics equation (*i.e.*, Eq. (1)) can be rewritten following Su *et al.* [32]

$$\begin{bmatrix} \{\mathcal{W}\} \ddot{\boldsymbol{\xi}} \\ \{\mathcal{B}\} \ddot{\boldsymbol{\nu}} \end{bmatrix} = \begin{bmatrix} \frac{1}{m} \{\mathcal{W}\} \mathbf{R}_{\{\mathcal{B}\}} & 0 \\ 0 & \{\mathcal{B}\} \mathbf{J}^{-1} \end{bmatrix} \mathbf{u} + \begin{bmatrix} \{\mathcal{B}\} \mathbf{J}^{-1} \{\mathcal{B}\} \boldsymbol{\tau}_g \\ g \hat{\mathbf{z}} \end{bmatrix}. \quad (14)$$

We design the feedback-linearization controller as

$$\mathbf{u}^d = \begin{bmatrix} m \{\mathcal{W}\} \mathbf{R}_{\{\mathcal{B}\}}^T & \mathbf{0} \\ \mathbf{0} & \{\mathcal{B}\} \mathbf{J} \end{bmatrix} \left(\begin{bmatrix} \mathbf{u}_\xi \\ \mathbf{u}_\nu \end{bmatrix} - \begin{bmatrix} g \hat{\mathbf{z}} \\ \{\mathcal{B}\} \boldsymbol{\tau}_g \end{bmatrix} \right), \quad (15)$$

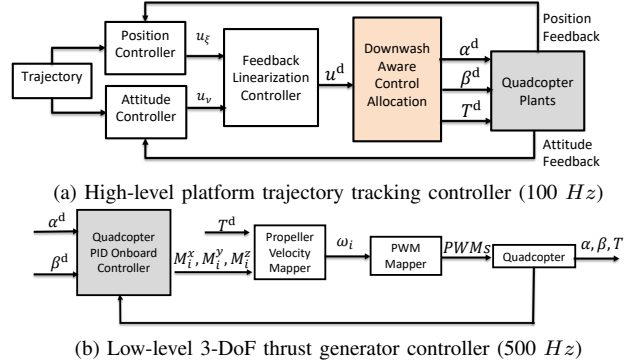


Fig. 4: Hierarchical control architecture. (a) The high-level position and attitude tracking controller gives desired 6-DoF wrench command \mathbf{u}^d to the downwash-aware control allocation through feedback linearization. \mathbf{u}^d is then allocated as the desired thrusts and joint angles for each 3-DoF thrust generator to maintain high thrust efficiency and avoid downwash effects. (b) In low-level control, each quadcopter module regulates its joint angles and thrust with an onboard PID controller. The angular velocity commands are converted to PWM signals for motor actuation.

where the subscript d indicates the desired values. Our above controller design transfers platform dynamics expressed by Eq. (14) into a simple double integrator [33]. Two virtual inputs \mathbf{u}_ξ and \mathbf{u}_ν can be designed with translational and rotational errors to track predefined reference position and attitude trajectory. We close this control loop by an LQR controller that considers communication delay and improves system robustness [33, 34].

B. Downwash-aware Control Allocation

The nullspace-based control allocation framework of over-actuated UAVs has been proposed in Su *et al.* [14] to solve $\boldsymbol{\alpha}$, $\boldsymbol{\beta}$, and \mathbf{T} from \mathbf{u}^d while maintaining defined input constraints. To avoid downwash effects and maintain high thrust efficiency, we modify the framework and reformulate the Quadratic Programming (QP) problem as described below.

An intermediate variable \mathbf{F} is defined as

$$\mathbf{F}(\boldsymbol{\alpha}, \boldsymbol{\beta}, \mathbf{T}) = [\mathbf{F}_1^T \quad \dots \quad \mathbf{F}_N^T]^T \in \mathbb{R}^{3N \times 1}, \quad (16)$$

where

$$\mathbf{F}_i(\alpha_i, \beta_i, T_i) = T_i \begin{bmatrix} \sin \beta_i \\ -\sin \alpha_i \cos \beta_i \\ \cos \alpha_i \cos \beta_i \end{bmatrix}. \quad (17)$$

With \mathbf{F} , we can transform the nonlinear allocation problem to a linear one,

$$\mathbf{u}^d = \begin{bmatrix} \mathbf{J}_\xi(\boldsymbol{\alpha}, \boldsymbol{\beta}) \\ \mathbf{J}_\nu(\boldsymbol{\alpha}, \boldsymbol{\beta}) \end{bmatrix} \mathbf{T} = \mathbf{W} \mathbf{F}, \quad (18)$$

where $\mathbf{W} \in \mathbb{R}^{6 \times 3N}$ is a constant allocation matrix with full row rank. Therefore, \mathbf{F} can be solved from \mathbf{u}^d with a general solution form,

$$\mathbf{F}(\boldsymbol{\alpha}, \boldsymbol{\beta}, \mathbf{T}) = \mathbf{W}^\dagger \mathbf{u}^d + \mathbf{N}_W \mathbf{Z}, \quad (19)$$

where $\mathbf{N}_W \in \mathbb{R}^{3N \times (3N-6)}$ is the nullspace of \mathbf{W} , and $\mathbf{Z} \in \mathbb{R}^{(3N-6) \times 1}$ is an arbitrary vector.

As discussed in Su *et al.* [14], Eq. (19) is linearized with the first-order Taylor expansion and relaxed with slack

variable $\mathbf{s} \in \mathbb{R}^{3N \times 1}$,

$$\mathbf{s} + \mathbf{F}(\mathbf{X}_0) + \frac{\partial \mathbf{F}}{\partial \mathbf{X}} \Big|_{\mathbf{x}=\mathbf{x}_0} \Delta \mathbf{X} = \mathbf{W}^\dagger \mathbf{u}^d + \mathbf{N}_W \mathbf{Z}, \quad (20)$$

where \mathbf{X} is defined as $\mathbf{X} = [\boldsymbol{\alpha}^\top, \boldsymbol{\beta}^\top, \mathbf{T}^\top]^\top$, $[\cdot]_0$ is the value of a variable at last time step, and $\Delta[\cdot]$ is the difference w.r.t. the previous time step of a variable.

Similarly, the downwash avoidance constraint (see Eq. (12)) can be approximated by another linear equation as a linear inequality constraint,

$$\mathbf{O}(\mathbf{X}_0) + \frac{\partial \mathbf{O}}{\partial \mathbf{X}} \Big|_{\mathbf{x}=\mathbf{x}_0} \Delta \mathbf{X} \geq \mathbf{O}_{\min}. \quad (21)$$

The physical constraints of the platform are designed as

$$\mathbf{X}_{\min} - \mathbf{X}_o \leq \Delta \mathbf{X} \leq \mathbf{X}_{\max} - \mathbf{X}_o, \quad (22)$$

$$\Delta \mathbf{X}_{\min} \leq \Delta \mathbf{X} \leq \Delta \mathbf{X}_{\max}. \quad (23)$$

The objective function is designed as

$$\Delta \mathbf{X}^\top \mathbf{Q}_1 \Delta \mathbf{X} + \mathbf{s}^\top \mathbf{Q}_2 \mathbf{s} + \mathbf{Z}^\top \mathbf{Q}_3 \mathbf{Z} + \mathbf{P}^\top \Delta \mathbf{X}, \quad (24)$$

where \mathbf{Q}_{1-3} are three positive semi-definite weighting matrices. As introduced in Section III-B, the thrust efficiency index is included as $\mathbf{P}^\top (\mathbf{X}_o + \Delta \mathbf{X})$, with

$$\mathbf{P}^\top = [\mathbf{0}_{1 \times 2N} \quad \gamma \mathbf{1}_{1 \times N}] \in \mathbb{R}^{1 \times 3N}. \quad (25)$$

Then we have

$$\mathbf{P}^\top (\mathbf{X}_o + \Delta \mathbf{X}) = \gamma \sum_{i=1}^N T_i, \quad (26)$$

where γ is the scaling factor. Of note, $\mathbf{P}^\top \mathbf{X}_o$ is a constant, thus removed from the objective function.

After solving this optimization problem Eqs. (20) to (24), we can approximately calculate the desired \mathbf{X} for next step with discrete integration,

$$\mathbf{X} = \mathbf{X}_o + \Delta \mathbf{X}. \quad (27)$$

To eliminate the approximation errors, we utilize nullspace projection with

$$\mathbf{Z}^* = \mathbf{N}_W^\dagger (\mathbf{F}(\mathbf{X}) - \mathbf{W}^\dagger \mathbf{u}^d), \quad (28)$$

$$\mathbf{F}^* = \mathbf{W}^\dagger \mathbf{u}^d + \mathbf{N}_W \mathbf{Z}^*. \quad (29)$$

Finally, with exact solution \mathbf{F}^* , low-level commands $\boldsymbol{\alpha}^d, \boldsymbol{\beta}^d$, and \mathbf{T}^d can be recovered with inverse kinematics:

$$T_i^d = \sqrt{F_{ix}^2 + F_{iy}^2 + F_{iz}^2}, \quad (30)$$

$$\alpha_i^d = \text{atan2}(-F_{iy}, F_{iz}), \quad (31)$$

$$\beta_i = \text{asin}\left(\frac{F_{ix}}{T_i}\right). \quad (32)$$

C. Low-level Control

The joint angles of each quadcopter module are controlled by separate PID controllers based on the error dynamics:

$$\begin{aligned} \ddot{\alpha}_i^d &= k_{P\alpha} e_\alpha + k_{I\alpha} \int e_\alpha dt + k_{D\alpha} \dot{e}_\alpha, \\ \ddot{\beta}_i^d &= k_{P\beta} e_\beta + k_{I\beta} \int e_\beta dt + k_{D\beta} \dot{e}_\beta, \end{aligned} \quad (33)$$

where $k_{[\cdot]\alpha}$ and $k_{[\cdot]\beta}$ are constant PID gains, and $e_\alpha = \alpha_i^d - \alpha_i^e$, $e_\beta = \beta_i^d - \beta_i^e$, are error terms with joint angle feedback α_i^e, β_i^e from onboard IMU. The related torque commands are determined by

$$\begin{aligned} M_i^x &= {}^B J_i^x \ddot{\alpha}_i^d \cos \beta_i, \\ M_i^y &= {}^B J_i^y \ddot{\beta}_i^d, \\ M_i^z &= {}^B J_i^z \ddot{\alpha}_i^d \sin \beta_i. \end{aligned} \quad (34)$$

For each quadcopter module, with Eqs. (6) and (7), the angular velocity $\omega_{i,j}$ of each propeller can be calculated, later converted to the PWM signal to drive the motor.

V. SIMULATION AND EXPERIMENT SETUPS

A. Simulation Setup

Before conducting experiments, we develop a simulation platform in Matlab Simulink/Simscape to evaluate and characterize the proposed downwash-aware control allocation framework. In addition to the UAV's physical parameters obtained from system identification, the dynamics of propeller motors and saturation, control frequencies, measurement noise, communication noise and delays, the simulator also incorporates the downwash aerodynamics model introduced in Section II-C based on experimental data.

The proposed allocation framework was verified on two over-actuated platforms with four and six 3-DoF thrust generators, respectively. Table I summarizes the physical and software properties acquired from the physical system used in simulation, where m_0 and I_0 refer to the mass and inertia matrix of the mainframe, and m_i and I_i refer to the mass and inertia matrix of each 3-DoF thrust generator.

TABLE I: Physical and Software Properties in Simulation

Parameter	Four	Six
m_0/kg	0.020	0.030
m_i/kg	0.050	0.036
$\text{diag}(I_0)/kg \cdot cm^2$	[3.20 3.20 4.70]	[4.50 4.50 6.20]
$\text{diag}(I_i)/kg \cdot cm^2$	[0.35 0.35 0.55]	[0.16 0.16 0.29]
l/m	0.21	0.18
a/m	0.068	0.032
t_{max}/N	0.30	0.15
Communication delay/sec	0.02	0.02
Remote PC control rate/Hz	100	100
Onboard control rate/Hz	500	500

B. Experiment Setup

As shown in Fig. 5, the quadcopters are connected to the central frame by 2-DoF passive gimbal mechanism, which have no rotation-angle limitations, thus can be utilized as 3-DoF thrust generators. We use Crazyflie 2.1 as the quadcopter module. The weight of Crazyflie 2.1 is 27g with a maximum 60g total payload. For the platform with four 3-DoF thrust generators, we upgraded the motors, propellers, and batteries of the Crazyflie for larger thrust force.

In the experiment, we use the Noitom motion capture system to measure the position and attitude of the central frame. The main controller runs on a remote PC, which communicates with the motion capture system through Ethernet. The main controller calculates the desired thrust \mathbf{T}^d ,

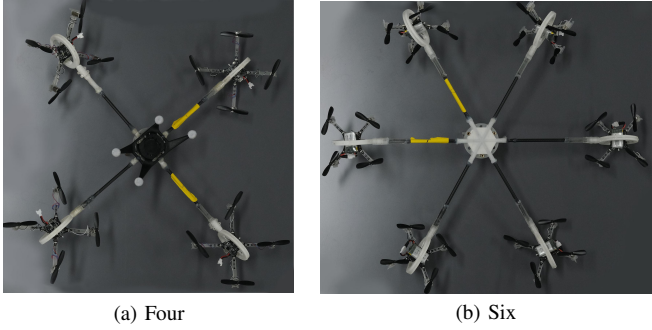


Fig. 5: Hardware prototypes of the over-actuated UAV platforms. The central frame is a rigid body made by carbon-fiber tubes and 3-D printed parts. Commercial quadcopter Crazyflie 2.1 from Bitcraze is combined with 3-D printed 2-DoF passive gimbal mechanism as the 3-DoF thrust generator. The platforms have (a) four and (b) six thrust generators, respectively.

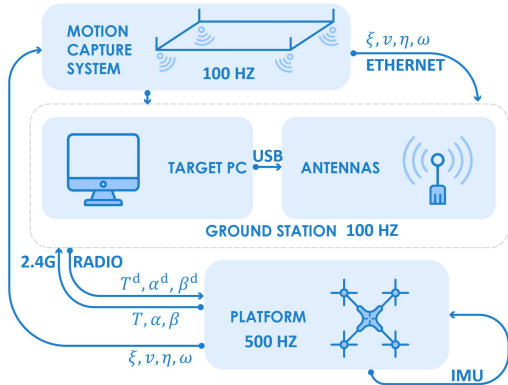


Fig. 6: Platform communication setup in experiment. The remote PC takes position and attitude feedback from motion capture system, runs the high-level controller, and sends commands to each quadcopter through radio communication.

tilting angles α^d , and twisting angles β^d for all quadcopter modules. The communication between the remote PC and each quadcopter is achieved by Crazy Radio PA antennas (2.4G Hz). Each quadcopter is embedded with an onboard IMU module, estimating the rotation angle given the attitude of central frame η . Meanwhile, the onboard controller regulates the tilting and twisting angles to desired values and provides the required thrust. The measurement rate of the motion capture system, the remote PC controller, and the data communication with each quadcopter are all set to 100 Hz. The quadcopter's onboard controller is set to 500 Hz for fast low-level response. Fig. 6 shows the software architecture.

VI. SIMULATION AND EXPERIMENT RESULTS

A. Simulation Results

Fig. 7 summarizes the simulation results of two over-actuated UAV platforms with the proposed downwash effect model introduced in Section II-C. For the platform that has four 3-DoF thrust generators, a reference attitude trajectory is designed where the downwash effects occur twice (Fig. 7a). As we can see, the downwash effect first appears at about 9s, when the platform is rotated at 90 degree along the axis $[-\frac{\sqrt{2}}{2}, \frac{\sqrt{2}}{2}, 0]$; T_4 and T_1 , as well as T_3 and T_2 , aligned

vertically (two pairs of downwash effect). With conventional allocation framework, the downwash flows significantly influence the control of the platform; we noticed a drop in Z axis with about 0.15 m, and the control performance of other 5-DoF is also deteriorated (Fig. 7b). Later, another downwash effect appears at about 16s (T_4 and T_2 aligned vertically), which finally makes the platform unstable. Using the proposed the downwash-aware allocation framework, the platform tracks the reference trajectory stably (Figs. 7f and 7g) and maintain a high thrust efficiency (Fig. 7h). Please see also Fig. 1 for better visualization.

For the platform that has six 3-DoF thrust generators, a 90 degree pitch reference trajectory (Fig. 7k) is utilized, and three pairs of downwash effects happen at the final altitude. With the conventional allocation framework, although the platform is still stable, we noticed a 0.3m drop in Z-axis with more than 5s to compensate for position control (Fig. 7l). Further, as we can see in Fig. 7m, this framework needs more thrusts to compensate for the downwash aerodynamics, inefficient in terms of energy. With our proposed downwash-aware allocation framework, the control in Z-axis is maintained, and the thrust is not increased by much for downwash avoidance. By exploring the entire allocation space, the downwash effects are avoided, and the high thrust efficiency is maintained.

B. Experiment Results

We conducted experiments on the over-actuated UAV platform that has four 3-DoF thrust generators to compare the conventional allocation framework and our proposed downwash-aware allocation framework; see Fig. 8. Using the conventional allocation framework, the platform is controlled to track a 90 degree pitch reference trajectory (Fig. 8a), where a pair of downwash effects appear, and an obvious drop in Z-axis is noticed (Fig. 8b). Although the uniformly high thrust efficiency is maintained by deploying all the thrusts in the same direction, this framework requires more thrust forces to slowly compensate downwash effects with the integrator of position controller (Fig. 8c). Moreover, the stability of the platform is influenced by more oscillations.

Using the proposed downwash-aware allocation framework, the platform avoids the downwash effects by deploying the proper thrust forces and maintains a high thrust efficiency (Figs. 8h to 8j). Therefore, the position and attitude tracking control performance is guaranteed along whole trajectory (Figs. 8f and 8g). Fig. 8k shows keyframes of the experiment.

C. Discussion

The minimum downwash avoid distance o_{min} in Algorithm 1 has to be experimentally decided for different platforms. $o_{min} = 0$ means the downwash avoidance is not activated. Large o_{min} may result in no feasible solution to the downwash-aware allocation problem. Despite that small o_{min} cannot fully avoid downwash flow, it still can improve the control performance to some extent. We chose $o_{min} = 7cm$ in the experiment.

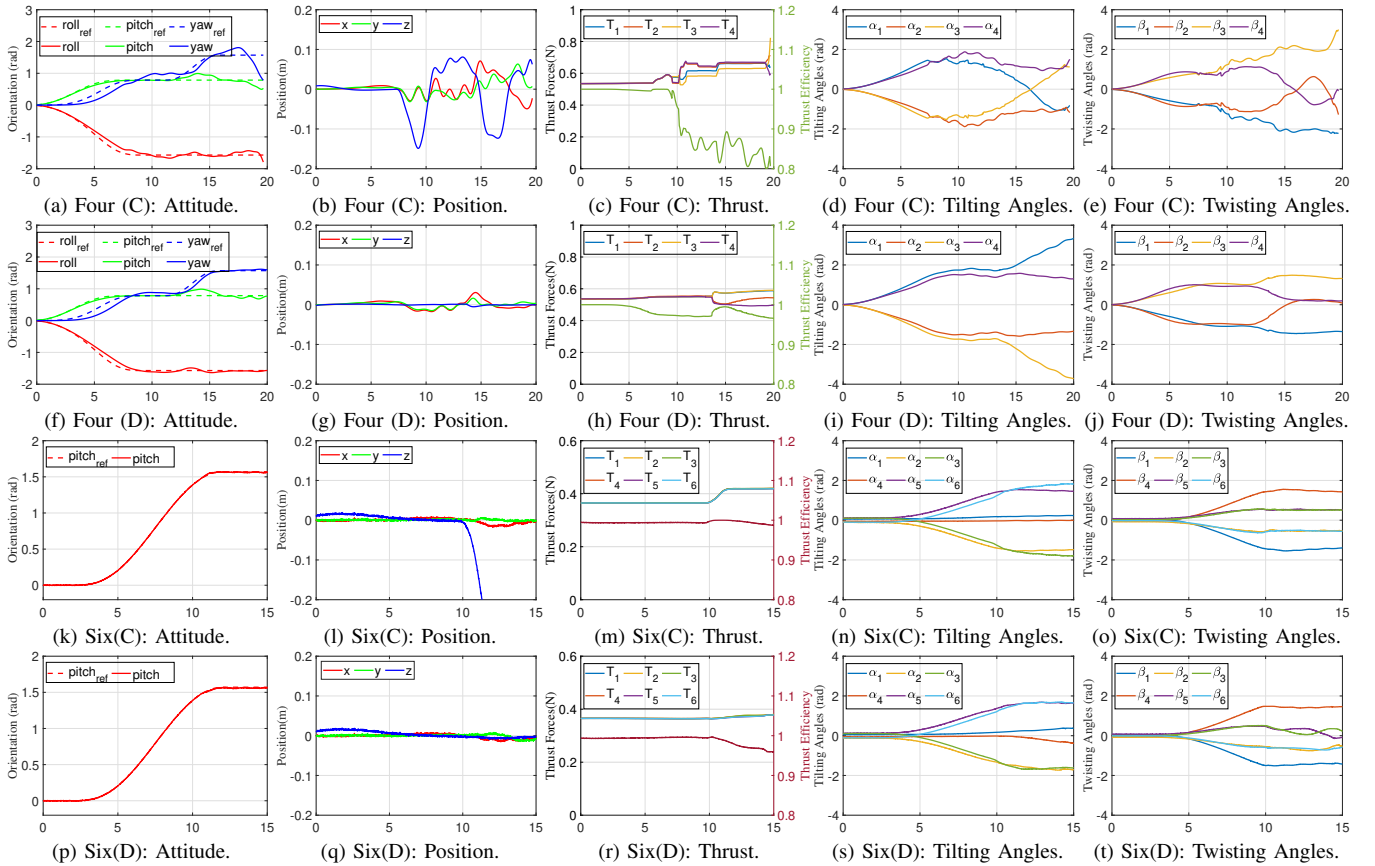


Fig. 7: **Simulation: Comparison of conventional and downwash-aware control allocation on two over-actuated UAV platforms.** C and D denotes conventional and downwash-aware control allocation, respectively.

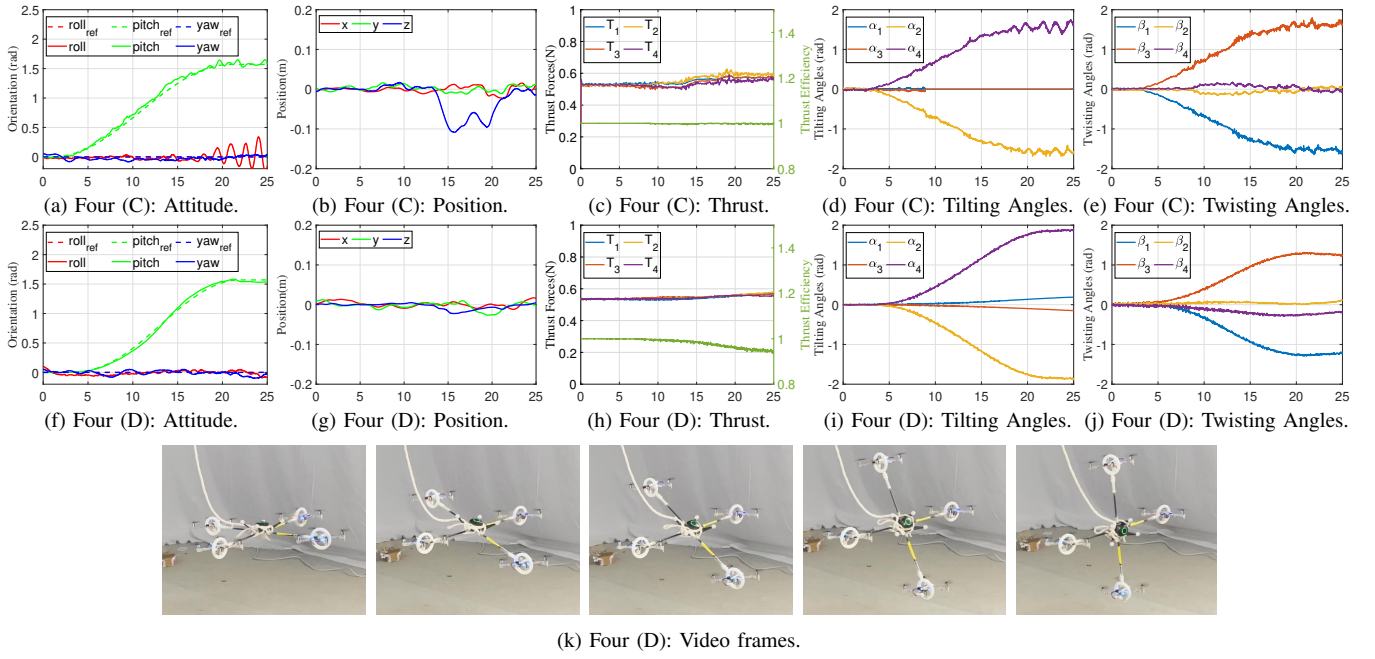


Fig. 8: **Experiment: Comparison of conventional and downwash-aware control allocation on the over-actuated UAV platform.**

VII. CONCLUSION

We presented the downwash-aware control allocation framework of over-actuated UAVs, which makes synergy of downwash effect avoidance and thrust efficiency main-

tenance. The downwash avoidance constraint and thrust efficiency index were derived and incorporated into the nullspace-based allocation framework. In simulation, the proposed downwash-aware and original nullspace-based allocation frameworks were studied and compared on two

different over-actuated platforms. These frameworks were further implemented on our customized UAV platforms in experiment for demonstration. Both simulation and experiment verified that our proposed framework fully explores the allocation space and finds the desired allocation solution that could both avoid downwash effect and maintain high thrust efficiency, significantly improving the control performance.

ACKNOWLEDGEMENT

The authors would like to thank Dr. Tengyu Liu, Nan Jiang, Zihang Zhao, Hao Liang, Zeyu Zhang, Zhen Chen, Yifei Dong at BIGAI for their constructive discussions and help on hardware design, motion capture system, and figures; Dr. Pengkang Yu at UCLA for his help on control framework of Crazyflie.

REFERENCES

- [1] T. Anzai, M. Zhao, X. Chen, F. Shi, K. Kawasaki, K. Okada, and M. Inaba, "Multilinked multirotor with internal communication system for multiple objects transportation based on form optimization method," in *Proceedings of International Conference on Intelligent Robots and Systems (IROS)*, 2017.
- [2] B. Li, L. Ma, D. Huang, and Y. Sun, "A flexibly assembled and maneuverable reconfigurable modular multi-rotor aerial vehicle," *IEEE/ASME Transactions on Mechatronics (TMECH)*, 2021.
- [3] M. J. Gerber and T.-C. Tsao, "Twisting and tilting rotors for high-efficiency, thrust-vectoring quadrotors," *Journal of Mechanisms and Robotics*, vol. 10, no. 6, p. 061013, 2018.
- [4] A. F. Şenkul and E. Altuğ, "System design of a novel tilt-roll rotor quadrotor uav," *Journal of Intelligent & Robotic Systems*, vol. 84, no. 1, pp. 575–599, 2016.
- [5] H.-N. Nguyen, S. Park, J. Park, and D. Lee, "A novel robotic platform for aerial manipulation using quadrotors as rotating thrust generators," *IEEE Transactions on Robotics (T-RO)*, vol. 34, no. 2, pp. 353–369, 2018.
- [6] C. Pi, L. Ruan, P. Yu, Y. Su, S. Cheng, and T. Tsao, "A simple six degree-of-freedom aerial vehicle built on quadcopters," in *Proceedings of IEEE Conference on Control Technology Applications (CCTA)*, 2021.
- [7] P. Yu, Y. Su, M. J. Gerber, L. Ruan, and T.-C. Tsao, "An over-actuated multi-rotor aerial vehicle with unconstrained attitude angles and high thrust efficiencies," *IEEE Robotics and Automation Letters (RA-L)*, vol. 6, no. 4, pp. 6828–6835, 2021.
- [8] N. Michael, D. Mellinger, Q. Lindsey, and V. Kumar, "The grasp multiple micro-uav testbed," *IEEE Robotics and Automation Magazine (RA-M)*, vol. 17, no. 3, pp. 56–65, 2010.
- [9] Y. Su, L. Ruan, P. Yu, C.-H. Pi, M. J. Gerber, and T.-C. Tsao, "A fast and efficient attitude control algorithm of a tilt-rotor aerial platform using inputs redundancies," *IEEE Robotics and Automation Letters (RA-L)*, vol. 7, no. 2, pp. 1214–1221, 2021.
- [10] H. Lee, M. Jeong, C. Kim, H. Lim, C. Park, S. Hwang, and H. Myung, "Low-level pose control of tilting multirotor for wall perching tasks using reinforcement learning," in *Proceedings of International Conference on Intelligent Robots and Systems (IROS)*, 2021.
- [11] W. Zhang, M. Brunner, L. Ott, M. Kamel, R. Siegwart, and J. Nieto, "Learning dynamics for improving control of overactuated flying systems," *IEEE Robotics and Automation Letters (RA-L)*, vol. 5, no. 4, pp. 5283–5290, 2020.
- [12] R. Yang, L. Zheng, J. Pan, and H. Cheng, "Learning-based predictive path following control for nonlinear systems under uncertain disturbances," *IEEE Robotics and Automation Letters (RA-L)*, vol. 6, no. 2, pp. 2854–2861, 2021.
- [13] P. Yu, *An Over-Actuated Multi-Rotor Aerial Platform and Iterative Learning Control Applications*. PhD thesis, University of California, Los Angeles, 2022.
- [14] Y. Su, P. Yu, M. Gerber, L. Ruan, and T.-C. Tsao, "Nullspace-based control allocation of overactuated uav platforms," *IEEE Robotics and Automation Letters (RA-L)*, vol. 6, no. 4, pp. 8094–8101, 2021.
- [15] W. Khan, M. Nahon, and R. Caverly, "Propeller slipstream model for small unmanned aerial vehicles," in *AIAA modeling and simulation technologies (MST) conference*, 2013.
- [16] Y. Zheng, S. Yang, X. Liu, J. Wang, T. Norton, J. Chen, and Y. Tan, "The computational fluid dynamic modeling of downwash flow field for a six-rotor uav," *Frontiers of Agricultural Science and Engineering*, vol. 5, no. 2, pp. 159–167, 2018.
- [17] K. P. Jain, T. Fortmuller, J. Byun, S. A. Mäkiharju, and M. W. Mueller, "Modeling of aerodynamic disturbances for proximity flight of multirotors," in *International Conference on Unmanned Aircraft Systems (ICUAS)*, 2019.
- [18] R. Miyazaki, R. Jiang, H. Paul, K. Ono, and K. Shimonomura, "Airborne docking for multi-rotor aerial manipulations," in *Proceedings of International Conference on Intelligent Robots and Systems (IROS)*, 2018.
- [19] J. L. Brinkman, B. Davis, and C. E. Johnson, "Post-movement stabilization time for the downwash region of a 6-rotor uav for remote gas monitoring," *Heliyon*, vol. 6, no. 9, p. e04994, 2020.
- [20] J. A. Preiss, W. Höning, N. Ayanian, and G. S. Sukhatme, "Downwash-aware trajectory planning for large quadrotor teams," in *Proceedings of International Conference on Intelligent Robots and Systems (IROS)*, 2017.
- [21] G. Shi, W. Höning, Y. Yue, and S.-J. Chung, "Neural-swarm: Decentralized close-proximity multirotor control using learned interactions," in *Proceedings of International Conference on Robotics and Automation (ICRA)*, 2020.
- [22] G. Shi, W. Höning, X. Shi, Y. Yue, and S.-J. Chung, "Neural-swarm2: Planning and control of heterogeneous multirotor swarms using learned interactions," *IEEE Transactions on Robotics (T-RO)*, 2021.
- [23] M. Ryll, H. H. Bülthoff, and P. R. Giordano, "A novel overactuated quadrotor unmanned aerial vehicle: Modeling, control, and experimental validation," *IEEE Transactions on Control Systems Technology*, vol. 23, no. 2, pp. 540–556, 2014.
- [24] M. Kamel, S. Verling, O. Elkhatib, C. Sprecher, P. Wulkop, Z. Taylor, R. Siegwart, and I. Gilitschenski, "The voliro omniorientational hexacopter: An agile and maneuverable tilttable-rotor aerial vehicle," *IEEE Robotics and Automation Magazine (RA-M)*, vol. 25, no. 4, pp. 34–44, 2018.
- [25] M. Zhao, K. Okada, and M. Inaba, "Enhanced modeling and control for multilinked aerial robot with two dof force vectoring apparatus," *IEEE Robotics and Automation Letters (RA-L)*, vol. 6, no. 1, pp. 135–142, 2020.
- [26] M. Santos, L. Honório, A. Moreira, M. Silva, and V. Vidal, "Fast real-time control allocation applied to over-actuated quadrotor tilt-rotor," *Journal of Intelligent & Robotic Systems*, vol. 102, no. 3, pp. 1–20, 2021.
- [27] T. A. Johansen, T. I. Fossen, and S. P. Berge, "Constrained nonlinear control allocation with singularity avoidance using sequential quadratic programming," *IEEE Transactions on Control Systems Technology*, vol. 12, no. 1, pp. 211–216, 2004.
- [28] M. A. da Silva Ferreira, M. F. T. Begazo, G. C. Lopes, A. F. de Oliveira, E. L. Colombini, and A. da Silva Simões, "Drone reconfigurable architecture (dra): A multipurpose modular architecture for unmanned aerial vehicles (uavs)," *Journal of Intelligent & Robotic Systems*, vol. 99, pp. 517–534, 2020.
- [29] M. Wang, Y. Su, H. Liu, and Y. Xu, "Walkingbot: Modular interactive legged robot with automated structure sensing and motion planning," in *Proceedings of International Symposium on Robot and Human Interactive Communication (RO-MAN)*, 2020.
- [30] L. Ruan, *Independent position and attitude control on multirotor aerial platforms*. PhD thesis, University of California, Los Angeles, 2020.
- [31] M. Ryll, D. Bicego, and A. Franchi, "Modeling and control of fast-hex: A fully-actuated by synchronized-tilting hexarotor," in *Proceedings of International Conference on Intelligent Robots and Systems (IROS)*, 2016.
- [32] Y. Su, *Compensation and Control Allocation with Input Saturation Limits and Rotor Faults for Multi-Rotor Copters with Redundant Actuators*. PhD thesis, University of California, Los Angeles, 2021.
- [33] L. Ruan, C. Pi, P. Yu, S. Cheng, Y. Su, and T. Tsao, "Control and experiments of a novel tiltable-rotor aerial platform comprising quadcopters and passive hinges," *Mechatronics (submitted)*, Elsevier, 2022.
- [34] Y. Su, P. Yu, M. Gerber, L. Ruan, and T. Tsao, "Fault-tolerant control of overactuated multirotor uav platform under propeller failure," *IEEE Transactions on Control Systems Technology (submitted)*, 2022.